

Overview on Turbulence and Structure Formation during Resonant Magnetic Perturbations at TEXTOR

Andreas Krämer-Flecken¹⁾, Yuhong Xu²⁾, Sergey Soldatov^{1,3)}, Marcin Jakubowski^{1,4)} Yungfeng Liang¹⁾, Dirk Reiser¹⁾ and Oliver Schmitz¹⁾

¹⁾ *Institute for Energy Research – Plasma Physics, Forschungszentrum Jülich, Association EURATOM-FZJ, Trilateral Euregio Cluster, Germany, www.fz-juelich.de/ief/ief-4*

²⁾ *Ecole Royale Militaire / Koninklijke Militaire School, Euratom-Belgian State Association, Trilateral Euregio Cluster, Avenue de la Renaissance 30, B-1000 Brussels, Belgium*

³⁾ *Nuclear Fusion Institute, RRC Kurchatov Institute, 123182, Moscow, Russian Federation*

⁴⁾ *Max-Planck-Institute for Plasma Physics, EURATOM-IPP Association, Greifswald, Germany*

(Received: 29 August 2008 / Accepted: 15 December 2008)

Resonant magnetic perturbations (RMPs) are discussed in ELM mitigation scenarios at different devices and envisaged for future devices as ITER. In parallel extensive efforts have been performed to measure and understand the interaction between turbulence and RMPs.

At TEXTOR poloidal cross correlation reflectometry, Mirnov coils and Langmuir probes are available to observe turbulent aspects during RMP operation. This paper will present an overview on different aspects of turbulence during application of RMPs. The presented investigations concentrate on (i) the reduction of the poloidal connection length due to formation of ergodic layers by the RMP on the geodesic acoustic mode at the plasma edge; (ii) the description of structures in RMP generated island chains and especially on the observation of flow patterns inside the island; (iii) the enhanced turbulent transport in the pump out scenario at TEXTOR and (iv) the effect of the RMP on the blobby transport at the plasma edge.

Keywords: Turbulent transport, resonant magnetic perturbation, geodesic acoustic mode, island structure, blobby transport

1. Introduction

During the last years extensive efforts have been performed to measure the turbulence characteristics and understand the interaction with resonant magnetic perturbations (RMPs). Turbulence and turbulent structures are the key for a better understanding of transport properties and a starting point for better control of particle- and energy transport with the aim to improve the plasma scenarios for future devices as ITER. As it was recently demonstrated at JET, the ELM activity can be mitigated by application of RMPs [1]. However, a deeper understanding of the interaction of RMPs with the plasma turbulence is needed.

At TEXTOR the tools to investigate the plasma – RMP interaction are available. To generate RMPs the dynamic ergodic divertor (DED) [2] is used. The large variety of different operation (3/1, 6/2 and 12/4) configurations allows to modify the magnetic topology at the plasma edge by varying the current in the perturbation coils, its frequency and the pulse shape. On the other hand TEXTOR is equipped with a set of different fast sampled and high resolution diagnostics, as poloidal correlation reflectometry (CR), reciprocating Langmuir probes and Mirnov coils. Those diagnostics have been successfully used in the study of

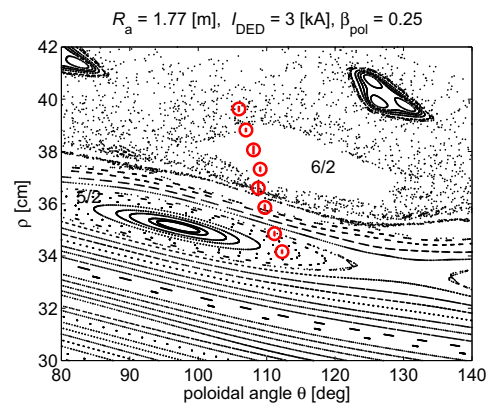


Fig. 1 Poincaré plot obtained for a vacuum calculation and a superimposed ohmic plasma with $q_a = 4.5$. The island chains of $m/n = 5/2$ and $m/n = 6/2$ are clearly visible.

zonal flows and GAMs [3], turbulence transport and blobby transport [4]. Since different plasma quantities are measured by these diagnostics, the correlation between them can yield additional information on the origin of turbulence itself.

In section 2 the DED and the different diagnostic tools are described. After a short overview on macroscopic effects and supposed structure formation at the edge in section 3, the influence of the RMP on the geodesic

author's e-mail: a.kraemer-flecken@fz-juelich.de

acoustic mode (GAM) is presented in section 4. Section 5 presents aspects of the structure in a RMP generated island chain. In section 6 the enhanced turbulent transport in the pump out scenario is discussed followed by section 7 on the blobby transport. Section 8 summarizes the observations and discusses the consequences for future applications of RMPs.

2. Diagnostic Tools at TEXTOR

TEXTOR ($R_o = 1.75$ m, $a = 0.46$ m) a limiter tokamak with circular poloidal cross section is equipped with a dynamic ergodic divertor [2] to generate RMPs. It consists of a set of 16 coils wrapped helically around the high field side of the vessel. The main resonances of the generated RMP can be set to $m/n = 3/1, 6/2$ and $12/4$. All here reported experiments are performed in the $6/2$ configuration with dc DED operation and varying DED current. Due to the RMP the plasma at the edge is not longer symmetrical in ϕ - and θ -direction, where ϕ and θ denote the toroidal and poloidal angle, respectively. Due to the applied RMP the nested flux surfaces at the edge become disturbed. Two different regions can be identified using the Kolmogorov length L_k in braided magnetic fields [5] as a measure. As long as the poloidal connection length (L_c) is less than the Kolmogorov length, the region is called laminar. If $L_c \gg L_k$ the region is called ergodic. The transition between laminar zone and ergodic layer takes place for $n_c \approx 3-4$, where n_c denotes the number of poloidal turns. In practice the laminar zone has a slab size of $\Delta r \approx 2$ cm depending on the plasma parameters and the DED current. A 4-channel correlation CR system [6] is available which measures density fluctuations and the perpendicular plasma rotation at two poloidal positions ($\theta = 0^\circ, 90^\circ$) with an array of 5 antennae at each position. It is further used to determine the turbulence decorrelation time and mean turbulence wavelength from poloidal distribution of the cross correlation coefficient. A set of Mirnov coils, $\Delta\phi = 135^\circ$ toroidally apart from the CR system, measures magnetic fluctuations at $\theta = 0^\circ, 30^\circ, 45^\circ, 60^\circ, 75^\circ, 90^\circ, 270^\circ$ and 330° . For the observation of the plasma potential and the ion saturation current at the plasma boundary multi-array Langmuir probes are installed on a fast reciprocating manipulator [7]. It allows the measurement of local electron temperature (T_e) and density (n_e) and the determination of the radial electric field (E_r) from the floating potential (ϕ_f).

3. General aspects of RMPs at TEXTOR

Effects of the DED on the plasma are recently presented in [8, 9]. For the knowledge of the position of island chains in 3-dim geometry and the relative position of the diagnostic with respect to the island

chains, Poincaré plots are of help. In Fig. 1 the magnetic structure at the position of the CR system for a plasma with fixed β_{pol} and I_{DED} is shown. The open circles indicate the positions of the CR cutoff layer for different probing frequencies, which are close to the RMP generated $m/n = 5/2$ island. Furthermore the

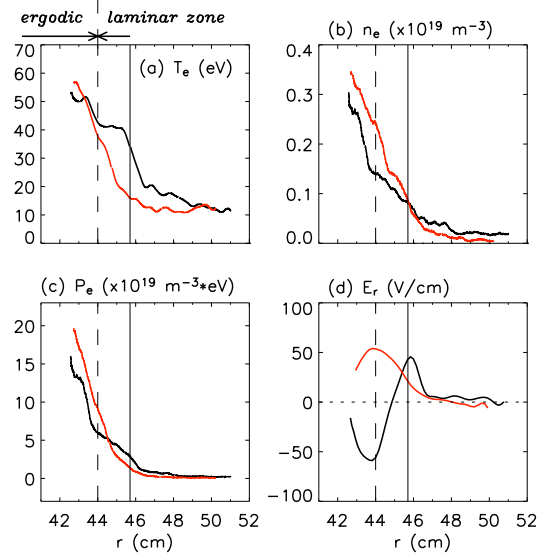


Fig. 2 Comparison of radial profiles from Langmuir probes for plasmas with RMP ($I_{DED} = 6$ kA) and without RMP: (a) T_e ; (b) n_e ; (c) p_e and (d) E_r .

$5/2$ island marks the region between open flux surfaces (ergodic layer) outside the island and intact surfaces more deep in the plasma.

Due to the short connection length to the target in the laminar region ($r \geq 0.44$ m) the turbulent spectrum changes. Coherent structures are reduced due to open field lines. The electron temperature (T_e) shows a significant reduction by a factor 2 (see Fig. 2a). In the ergodic region the decrease in T_e is much less pronounced compared to the laminar zone. The gradients in electron density (n_e) and plasma pressure (p_e) become more steep in the laminar zone (see Fig. 2c,d). The higher mobility of the electrons compared to the ions in this region of open field lines causes a faster loss of electrons and increases the floating potential ϕ_f , measured by probes. From two radial different measurements of ϕ_f the radial electric field E_r is calculated. In Fig. 2d the comparison of E_r with and without RMP is shown. Note that the maximum in E_r is shifted from the position of the last closed flux surface in a discharge without RMP to the position where the transition from the laminar to ergodic zone takes place. More deep in the plasma E_r decreases again. The change E_r is also obtained from the measurements of the perpendicular plasma velocity (v_\perp) by the CR system

$$E_r = -(v_\perp - v_{dia}) \cdot B_t \quad (1)$$

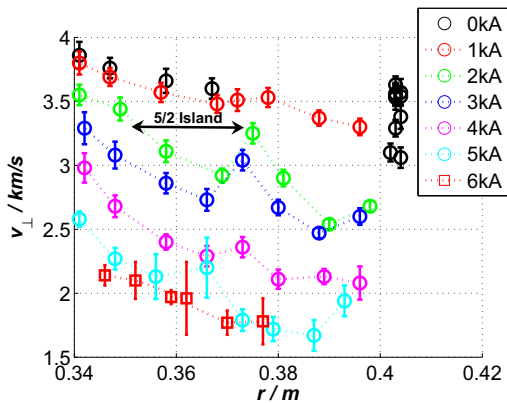


Fig. 3 Profiles of v_{\perp} for ohmic plasma at different I_{DED} generating the RMP.

where v_{dia} is the diamagnetic drift velocity. Furthermore the RMP has a large impact on the plasma rotation. The braking of the plasma by the RMP is seen in Fig. 3, where radial profiles of v_{\perp} are shown for different I_{DED} . A reduction of a factor 2, compared to the non DED case is observed in the ergodic zone for the highest I_{DED} current. Comparing the data for $I_{DED} = 3$ kA with the Poincaré plot in Fig. 1, a clear correlation between the hump in v_{\perp} at $r = 0.375$ m and the position of the $m/n = 5/2$ island is seen for $2 \leq I_{DED} \leq 4$ kA. The $5/2$ island width obtained from the calculations is indicated in Fig. 3 by a double arrow. The observed hump in v_{\perp} can be related to the outer separatrix of the $5/2$ island. Poincaré plots at $I_{DED} 4$ kA show a stronger ergodization which leads to the disappearance of the hump.

4. GAMs and RMP

Geodesic acoustic modes modulate or even suppress the ambient turbulence by means of zonal flows. The additional shearing of the rotation velocity [10] can act as a trigger mechanism to improved confinement. GAMs are predominately visible at the plasma edge where the effect of RMP is large. They show up in frequency spectra of different diagnostics as a single sharp line in the frequency range $10 \leq f_{GAM} \leq 25$ kHz. The frequency is a function of the local electron (T_e) and ion temperature (T_i). A further signature of GAMs is the long distance correlation e.g. for measurements with $\Delta\theta \geq 90^\circ$.

In several experiments the influence of RMPs on GAMs is studied. In these experiments the scaling of the GAM frequency with local temperature, the poloidal distribution, the density fluctuations and the velocity oscillations are investigated. Therefore the DED current is increased on a shot to shot basis by $\Delta I_{DED} = 1$ kA. For each pulse the CR system scans a radial range of $0.34 \leq r \leq 0.41$ m using the top antennae array. With increasing I_{DED} , the effect of

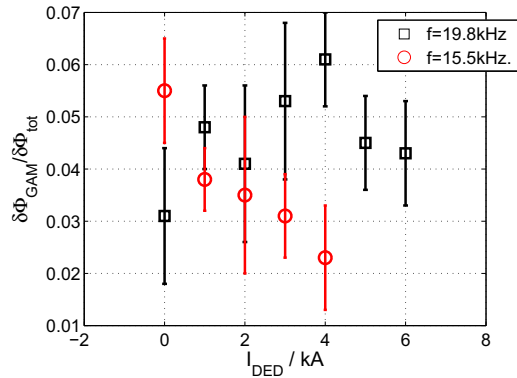


Fig. 4 Development of the relative phase fluctuations $\delta\Phi_{GAM}/\delta\Phi_{tot}$ for two frequencies with increasing RMP. Each frequency belongs to a different radius: (i) $f = 19.8$ kHz; $0.345 \leq r \leq 0.350$ m and (ii) $f = 15.5$ kHz; $0.380 \leq r \leq 0.385$ m.

the RMP on the plasma increases and the GAM disappears at the plasma edge, however, at $r = 0.34$ m a peak at $f = 19.8$ kHz is still visible for $I_{DED} = 6$ kA. The measured frequency agrees with the expected GAM frequency. The phase fluctuations measured by the CR system are proportional to the density fluctuations [13]. Fig. 4 shows the relative GAM induced phase fluctuation ($\delta\Phi_{GAM}/\delta\Phi_{tot}$) for two different frequencies. The frequencies belong to different radial positions. For $f = 15.5$ kHz, $\delta\Phi_{GAM}/\delta\Phi_{tot}$ decreases with I_{DED} . However, for $f = 19.8$ kHz which corresponds to $0.345 \leq r \leq 0.350$ m an increase in the amplitude is observed. This is the radial region where the $m/n = 5/2$ is assumed (see Fig. 1). A further test of the long distance correlation by measuring simultaneously with top and midplane antennae shows no correlation at the frequency at the innermost radius. This is an indication that the observed peak is not a GAM. A critical test for the GAM is the simultaneous measurement of GAM induced density fluctuations and the related velocity oscillations. It stems from the fact that an increase in the density fluctuation is related to an increase in the potential fluctuations [11, 12]:

$$\frac{\delta n_{GAM}}{n_c} \sim \frac{e\delta\phi_{GAM}}{T_e} \quad (2)$$

Here $\delta n_{GAM}/n_c$ denote the GAM induced relative density fluctuations, ϕ_{GAM} the potential fluctuations, T_e the electron temperature and e the electron charge. Since T_e does not change, an increase of $\delta n_{GAM}/n_c$ is related to an increase in ϕ_{GAM} which implies an increase in the $\tilde{E} \times B$ velocity oscillations. Since the reflection layer is fixed, any oscillation in $\tilde{v}_{E \times B}$ will show up in the measured fluctuation of the propagation time (δt) measured between two antennae. In Fig. 5 the phase fluctuation (a) and the related oscillation (b) are shown.

lations in the δt (b) are shown for $r = 0.347$ m for a case without RMP and a case with $I_{DED} = 4$ kA. For the phase fluctuations a clear increase with DED is seen but no increase in the velocity oscillations is visible. The phase fluctuations are not driven by the \widetilde{E}_r as it could be expected from the influence of the RMP on E_r . This indicates that the observed line at the GAM frequency is not a GAM.

In the stochastic region the decrease of the GAMs can be understood from the comparison of the poloidal connection length to the target and the distance traveled by particles within the time of a GAM oscillation. The GAM period at TEXTOR is in the order of $50 \leq T_{GAM} \leq 70 \mu\text{s}$. For thermal electrons at a local temperature of $100 \leq T_e \leq 300$ eV the propagation distance $l_p = v_{th} \cdot T_{GAM}$ within T_{GAM} yields 420 m to 500 m, where v_{th} denotes the thermal velocity. This has to be compared with the $L_c = n_c q 2\pi R_0$, where n_c is shown color coded in Fig. 6 and q denotes the local safety factor. With $330 \leq L_c \leq 400\text{m}$ for $12 \leq n_c \leq 14$, $L_c < l_p$ and therefore GAM oscillations are not possible.

The disappearance of the GAMs is also seen in the frequency spectrum of probe measurements [7], where an exponential decrease in the frequency range $f \leq 50$ kHz is observed for $I_{DED} = 6$ kA.

5. Structures in RMP generated Islands

As mention in section 4 the observed peak at a frequency close to the GAM frequency shows not the GAM properties. For several discharges with $q_a = 3.7$ and $I_{DED} = 6$ kA this line is investigated in detail. From a Poincaré plot (see Fig. 7), where the radial positions of the reflection layer for the probing frequency of the CR system are included, it can be seen that the estimation of v_{\perp} is close to the separatrix of the

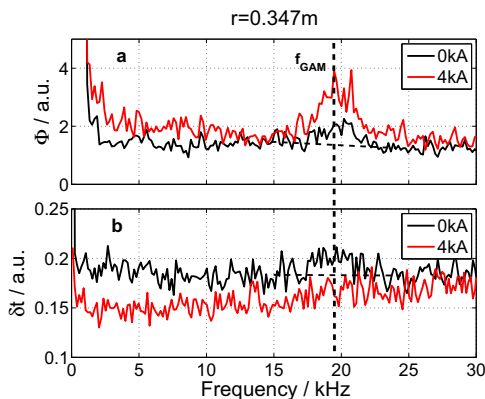


Fig. 5 Phase (Φ) and δt spectrum for $I_{DED} = 4$ kA. The increase in the Φ spectrum is seen clearly whereas no effect in the δt spectrum is seen. The black dashed lines indicate the background level for the reference case

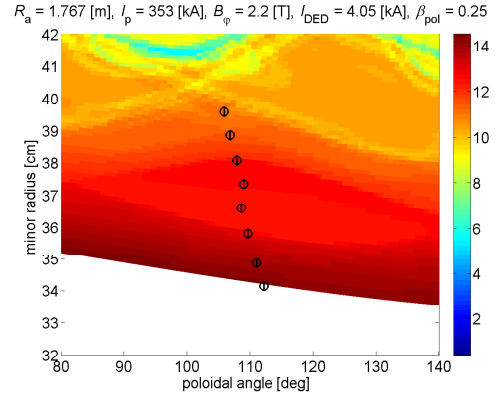


Fig. 6 The color coded poloidal turns n_c to reach the target. Black circles denote the poloidal position of the cutoff layer of the CR-system.

$5/2$ island. The CR-system covers the transition from the ergodic zone to the inner plasma where $L_c \rightarrow \infty$. At the outer separatrix a frequency of 19.8 kHz is ob-

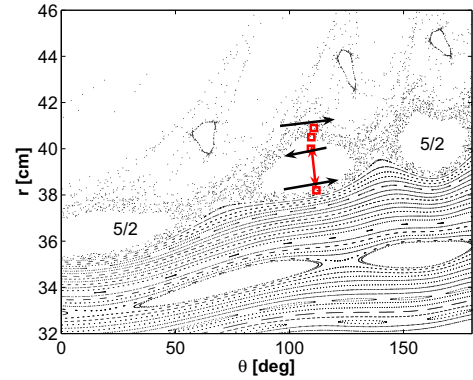


Fig. 7 Poincaré Plot with reflection layer of the CR system for $I_{DED} = 6$ kA. The red arrow indicates the radial elongation of the reflection layer. Black arrows indicate the rotation direction in the island.

served. Increasing the probing frequency a further line at 23.2 kHz shows up. At the innermost position the measurement is already outside the island and both lines have disappeared. However, the ion temperature gradient driven quasi coherent mode is observed in the coherence spectrum which is a further indication that the measurement is already outside the $5/2$ island. In the island itself a constant density is assumed, so that the measurement showing both lines is representative for the whole island width (indicated by the double arrow across the island), due to the reduction in radial resolution of the CR-system. The observations are in agreement with a poloidal flow inside the island [14]. From the observed frequency gap detected by the CR system and the assumption of a closed flow in the island, it will be once in the direction of the plasma perpendicular rotation (Ω_{\perp}) and once antiparallel.

From the CR-system Ω_{\perp} is deduced for the ambient plasma (without the 19.8 kHz line) and yields $\Omega_{\perp} = 10.1$ krad/s. This corresponds to a measured frequency difference of $10.1/\pi = 3.2$ kHz, which is exactly the difference between the two frequency bands. Since the 23.2 kHz line is observed more deep in the plasma the flow inside the island and the plasma rotation must be parallel. For the the 19.8 kHz line plasma rotation and flow in the island are antiparallel (see also the arrows in Fig. 7).

Rotating magnetic fluctuations, connected with the island structure, are detectable by Mirnov coils. The

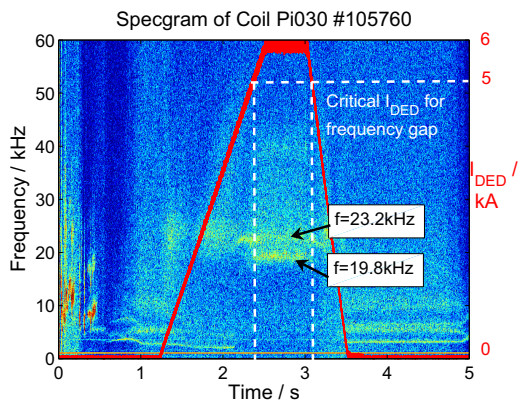


Fig. 8 Spectrogram of a Mirnov coil at 30° . Overlaid is the DED current. For $I_{DED} \geq 5$ kA (denoted at the right axis) two frequency bands are observed.

different toroidal position ($\Delta\phi = 135^{\circ}$) with respect to the CR-system gives further insight in the magnetic structure generated by the RMP. Looking at a Mirnov coil signal during ramp up of I_{DED} (Fig. 8) shows broad band fluctuations centered at $f \approx 25$ kHz. At a threshold of $I_{DED} = 5$ kA two sharp bands are observed with the above mentioned frequencies. This threshold can be related to the formation of a $5/2$ island with a certain width. This can be verified experimentally by decreasing either the DED current or increasing q_a which will decrease the influence of the RMP on the island. In both cases the observed frequency bands should disappear, which indeed is the case.

Upper and lower frequency are a measurement of a secondary structure in the $5/2$ island [15]. Further evidence for this assumptions is found from the estimation of the cross correlation between a top antennae of the CR system and different poloidal Mirnov coils. They show a strong correlation at 19.8 kHz and 23.2 kHz (see Fig. 9). Note that for $t \approx 2.1$ s a step of $\Delta f = 1$ GHz in the CR system moves r_c more inward, thus covering the whole island, and detects beside the 19.8 kHz line also a line at 23.2 kHz. Knowing the rotation direction of the background plasma, which is in electron diamagnetic drift (edd) direction the rotation

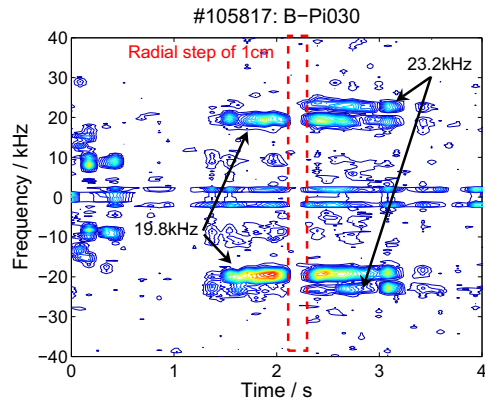


Fig. 9 Cross correlation between antennae B on top and Mirnov coil at 30° . Note that the 23.2 kHz line is more inside located than the 19.8 kHz line.

of the flow inside the island is ion diamagnetic drift (idd) direction. The different poloidal rotation directions are also seen in Fig. 9, where the color coded coherence for -19.8 kHz line is dominating (edd direction) compared to the 19.8 kHz line. The 23.2 kHz line (idd direction) is more pronounced than the -23.2 kHz line. Furthermore looking at the cross phase between two antennae at the 19.8 kHz line a strong deviation from the ambient rotation is found which indicates no or only small perpendicular rotation. This is in agreement with a set of closed surfaces in the island, as expected in a developed island.

6. Turbulent Transport in Pump Out Scenario

A special case of the RMP application at TEXTOR is the pump out scenario, where the RMP yields a 10-20% reduction in the line averaged density. Also a reduction in the effective particle confinement time (τ_p^*) is found. To find the region of enhanced transport, the turbulence properties in this scenario are analyzed. Therefore the decorrelation time $\tau_{DC} = \theta_{FWHM} \cdot r/v_{\perp}$ and the mean perpendicular wavelength $\langle\lambda_{\perp}\rangle = 2\pi \cdot r_c/\zeta_{FWHM}$, where θ_{FWHM} and ζ_{FWHM} denote the full width at half maximum of the poloidal distribution of the cross and auto correlation function, respectively, as obtained from different antenna combinations of the CR-system [3]. Whereas $\langle\lambda_{\perp}\rangle$ does not change with the RMP a strong decrease in τ_{DC} is observed during RMP operation. This decrease is observed more less for the complete radial range under investigation. A significant reduction from $12 \mu\text{s}$ without DED to $7 \mu\text{s}$ is observed during DED operation. Assuming a turbulent transport coefficient based on a simple random walk approach:

$$D_{turb}^{RW} \sim \frac{\langle\lambda_{\perp}\rangle^2}{\tau_{DC}} \quad (3)$$

an increase by $\approx 50\%$ is obtained (see Fig. 10).

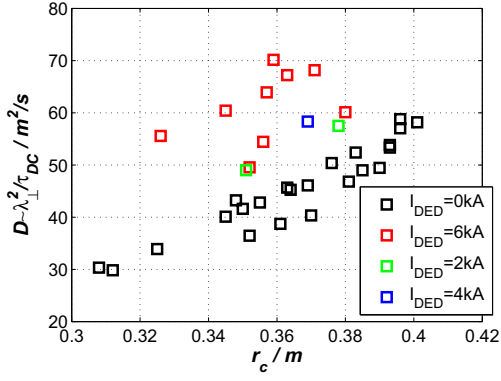


Fig. 10 Increase of $D_e^{RW} \tau_{DC}^{RW}$ during RMP operation in the pump out scenario for different values of I_{DED}

7. Blobby Transport

The transport in the scrape of layer (SOL), measured with a reciprocating probe, exhibits intermittency behaviour caused by the abrupt transition from closed to open flux surfaces. Due to the $E \times B$ transport, blobs, generated at the last close flux surface (LCFS), move into the SOL by 1–2 cm. With the application of RMPs the blob transport is reduced [16]. Fig. 11 a,e shows a reduction in the ion saturation current $I_s \propto \tilde{n}_e \sqrt{T_e}$ during RMP application. From Fig. 11 b,f it can be seen that v_r is not much changed during RMP operation. Comparing the radial particle flux $\Gamma_r = \langle \tilde{n}_e \tilde{v}_r \rangle$ in Fig. 11 c,g a reduction in Γ_r by the blobs is observed, when a RMP is applied and which agrees with simulations [17], where it is shown that the radial $E \times B$ transport is reduced outside the last closed flux surface and the mean propagation length is reduced, thus the blob cannot move into the SOL.

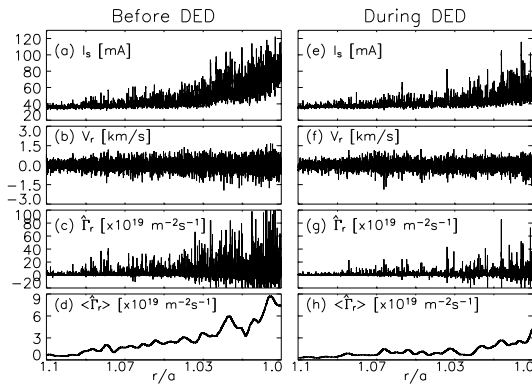


Fig. 11 Comparison of I_s , v_r and Γ_r in the SOL before and during RMP application.

8. Discussion and Conclusion

The paper gives an overview on different aspects of resonant magnetic perturbations, applied at TEX-

TOR plasmas. Due to laminar and ergodic zones with open stochastic field lines electron losses become dominant and generate a positive E_r at the plasma edge. Also the plasma rotation is effectively reduced over a large radial range.

The open and stochastic field lines forestall the generation of geodesic acoustic modes at the plasma boundary. The measured propagation length for the GAMs is larger than the connection length to the target. Since GAMs and zonal flows are discussed as a trigger for a transition to improved confinement, in that sense RMPs are not favorable.

A flow in the 5/2 island chain is observed. The obtained frequency gap is explained by the superposition of the flow inside the island with the flow in the surrounding plasma. In addition indications for secondary structures in the island are found.

The turbulence in the ergodic region is investigated in the density pump out scenario. A significant decrease in the decorrelation time of the turbulence is found. The estimated turbulence wavelength is not changed. The random walk turbulent diffusion coefficient is therefore enhanced by $\approx 50\%$ in the ergodic region. This may be the explanation for the decrease in τ_p^* .

In the SOL a reduction of blob transport with the application of the RMP is found based on reduced radial $E \times B$ transport outside the LCFS. This could be beneficial for the plasma wall interaction.

Acknowledgment This work is performed under the INTAS contract 1000008-8046.

- [1] Y. Liang et al., Phys. Rev. Lett., **98**, 265004, (2007)
- [2] K.H. Finken et al., Fusion Eng. Des., **37**, (1997), p 335
- [3] A. Krämer-Flecken et al., Phys. Rev. Lett., **97**, 045006, (2006)
- [4] Y. Xu et al., Phys. Rev. Lett., **97**, 165003, (2005)
- [5] I. Kaganovich, V. Rozhansky, Phys. of Plasmas, **5** (1998), pp 3901-3909
- [6] A. Krämer-Flecken et al., Nucl. Fusion, **46**, (2006), pp S730-S742
- [7] Y. Xu et al., Nucl. Fusion, **47**, (2007), pp 1696-1709
- [8] K.H. Finken et al., Nucl. Fusion, **47**, (2007), pp 522-534
- [9] M. W. Jakubowski et al., Plasma Phys. Control. Fusion, **49**, (2007), S109-S121
- [10] K. Itoh et al., Physics of Plasmas **13**, 055502 (2006)
- [11] P. Diamond et al., Plasma Phys. Control. Fusion, **47**, (2005), R35
- [12] T. Ido et al., Plasma Phys. Control. Fusion, **48**, (2006), pp S41-S50
- [13] A. Krämer-Flecken et al., Nucl. Fusion, **44**, (2004), pp 1143-1157
- [14] K. Ida et al., Nucl. Fusion, **44**, (2004), pp 290-295
- [15] Y. Liang et al., Nucl. Fusion, **47**, (2007), pp L21-L25
- [16] Xu et al., 35th EPS, Hersonissos, Crete, Greece, June 9-13, 2008, O-4.052,
- [17] D. Reiser, Phys. Plasmas, **14**, 082314, (2007)